Supporting Information

Interlayer Defect Promoting Phosphate Group Doping into TiO_2(B) Nanowires with Unusual Structure Properties toward Ultra-Fast and Ultra-Stable Sodium Storage

Meiling Kang [a, #], *Yurong Ruan* [a, #], *Lan Luo*[a], *Yanzhong Lu*[a], *Jinxian Huang*[a], *Jian-Min Zhang** [a] and *Zhensheng Hong** [a, b]

[a] Fujian Provincial Key Laboratory of Quantum Manipulation and New Energy Materials, College of Physics and Energy, Fujian Normal University, Fuzhou, Fujian 350117, China
[b] Fujian Provincial Collaborative Innovation Center for Optoelectronic Semiconductors and Efficient Devices, Xiamen, 361005, China
E-mail: jmzhang@fjnu.edu.cn (J. M. Zhang); winter0514@163.com (Z. Hong)
[#]These authors contributed equally to this work

1. Experimental Section

1. Characterizations of the samples

The crystal phase of the electrode materials were characterized by X-ray diffraction (XRD) by a equipment of Rigaku Ultima IV diffract meter, which adopts Cu Ka radiation. The morphology of the nanowires was observed by using the Scanning electron microscopy (SEM) by S8010 instrument) and transmission electron microscopy (TEM) by FEIF20 S-TWIN instrument. The analysis of X-ray photo-electron spectroscopy (XPS) was conducted by a PHI Quantum2000 XPS system.

2. Electrochemical measurement

The slurry was fabricated through mixing electrode materials, super P and Gum Arabic (GA) binder with weight ratio of 7:2:1. GA was dissolved in deionized water with a concentration of 30 mg ml^{-1}. Copper foil cut into circular piece was used as collector, which was coated with slurry, and then dried at 120 ^oC under vacuum condition for 12 h. Sodium ion batteries were assembled in a coin-type cells (CR 2025) with sodium foils as a counter electrode, glass fiber separator (Whatman GF/F), and 1 M $NaPF_6$ in diethylene glycol dimethyl ether (DEGDME) as the electrolyte. The Na metal foil, working electrode, and glass fiber separator (Whatman GF/F) were punched into circular sheets with diameters of 1.4 cm, 1.2 cm and 1.6 cm respectively, and then assembled in glove box filled with Ar atmosphere. The charge/discharge measurements of the batteries were performed on

Land CT2001A testers (Wuhan, China) between 2.5 and 0.01 V at room temperature at various current densities. Cyclic voltammogram (CV) measurements and electrochemical impedance spectroscopy (EIS) were conducted on a Zennium (Zahner). The GITT measurements were conducted using a current density of 0.1 A/g for 10 min between rest intervals for 2 h.

3. Theoretical Calculation

First-principles calculations were performed using the Vienna ab initio simulation package (VASP)[1, 2]. The exchange–correlation functions were treated within the generalized gradient approximation (GGA) of the Perdew-Burke-Ernzerhof type (PBE)[3-5]. The cut-off energy of plane-wave was set to 500eV for all calculations. A Monkhorst−Pack 3×7×3 k-point mesh for the Brillouin zone sampling of 1×1×2 TiO_2-B supercells, and all the atoms were fully relaxed until Hellmann−Feynman forces on each atom was less than 0.02eV/ Å. The GGA+U was adopted with the Dudarev's approach[6] for electronic structures and total energy calculations, and the on-site Hubbard U for the correlated Ti-3d with U_f=4.2eV[7, 8]. The minimum energy paths and activation energy for Na diffusion were calculated with the climbing image nudged elastic band (CI-NEB) method[9]. In order to avoid mixing of the diffusion barrier with the charge transfer barrier, we used the standard GGA instead of GGA+U for CI-NEB calculation[10]. The Na diffusion in the bulk and surface was calculated using 1×2×2 supercells and 1×2 supercell of TiO_2(B) (001) slab, respectively. For TiO_2(B) (001) slab, a vacuum buffer space of 15Å was added alone c-axis in calculations.

References

1. Kresse G; Hafner J. Ab initio molecular dynamics for open-shell transition metals. *Phys. Rev. B.* **48**, 13115-13118 (1993).

2. Kresse G; Furthmüller J. Efficient iterative schemes for ab initio total-energy calculations using a plane-wave basis set. *Phys. Rev. B.* **54**, 11169-11186 (1996).

3. Kresse G; Furthmüller J. Efficiency of ab-initio total energy calculations for metals and semiconductors using a plane-wave basis set. *Comput. Mater. Sci.* **6**, 15-50 (1996).

4. Perdew J. P; Burke K; Ernzerhof M. Generalized gradient approximation made simple. *Phys. Rev. Lett.* **77**, 3865-3868 (1996).

5. Blöchl P. E; Projector augmented-wave method. *Phys. Rev. B.* **50**, 17953-17979 (1994).

6. Dudarev S. L; Botton G. A; Savrasov S. Y; Humphreys C. J. & Sutton A. P. Electron-energy-loss spectra and the structural stability of nickel oxide: An LSDA+ U study. *Phys. Rev. B.* **57**, 1505-1509 (1998).

7. Morgan B. J; Watson G. W. A DFT^{+}U description of oxygen vacancies at the TiO_2 rutile (110) surface. *Surf. Sci.* **601**, 5034-5041 (2007).

8. Morgan B. J; Watson G. W. A density functional theory+ U study of oxygen vacancy formation at the (110), (100), (101), and (001) surfaces of rutile TiO_2. *J. Phys. Chem. C.* **113**, 7322-7328 (2009).

9. Henkelman G; Uberuaga B. P; Jónsson H. A climbing image nudged elastic band method for finding saddle points and minimum energy paths. *J. Chem. Phys.* **113**, 9901-9904 (2000).

10. Ong S. P; Chevrier V. L; Hautier G; Jain A; Moore C; Kim S; Ma X; Ceder G. Voltage, stability and diffusion barrier differences between sodium-ion and lithium-ion intercalation materials. *Energy Environ. Sci.* **4**, 3680-3688 (2011).

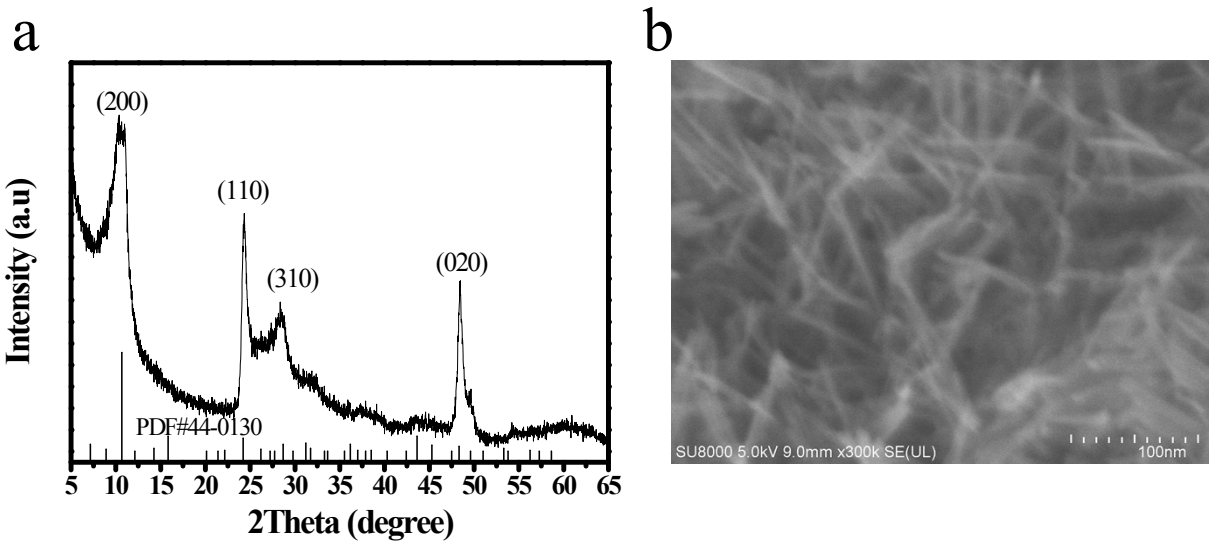

Fig. S1 (a) XRD and (b) SEM image of H-titanate nanowires.

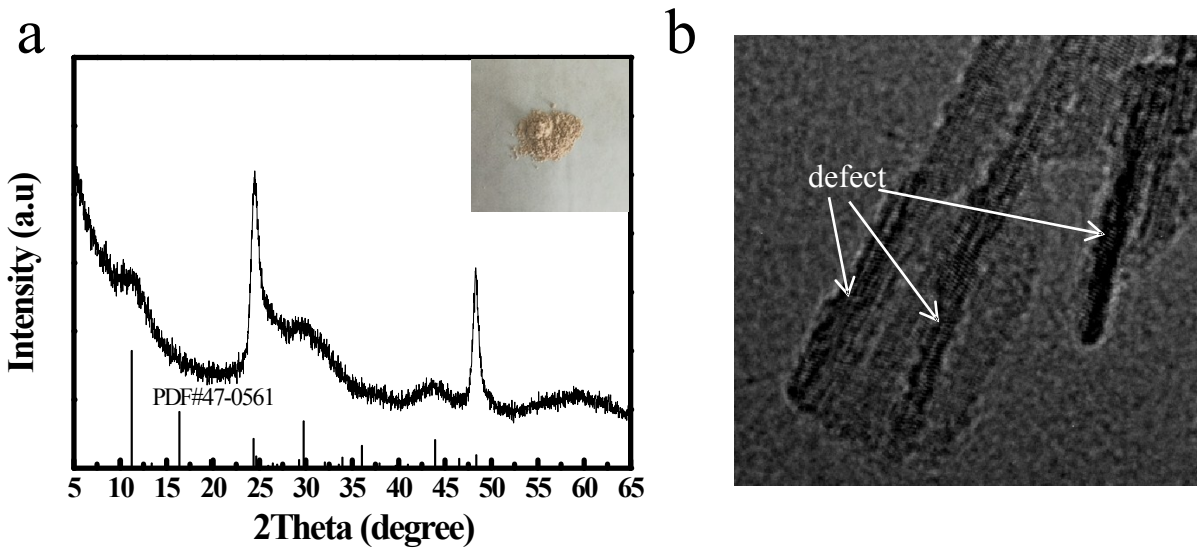

Fig. S2 (a) XRD and (b) HRTEM image of the intermediate phase during sintering.

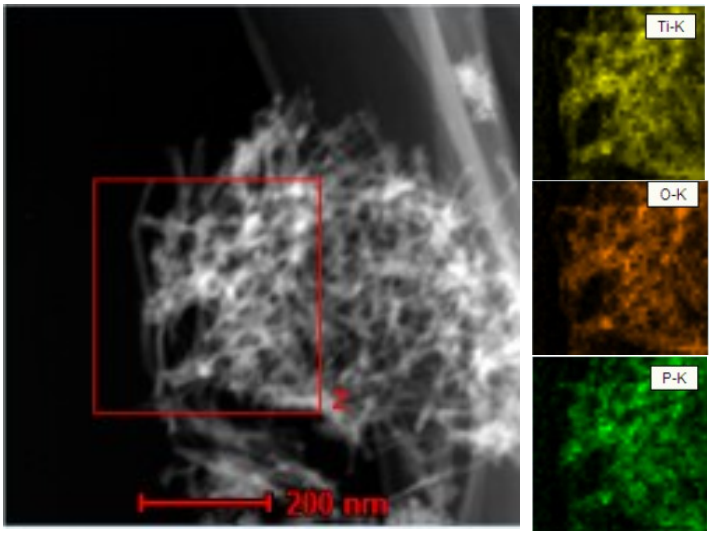

Fig. S3 Corresponding EDX elemental mapping Ti, O, and P of B-TiO_2(B)-P.

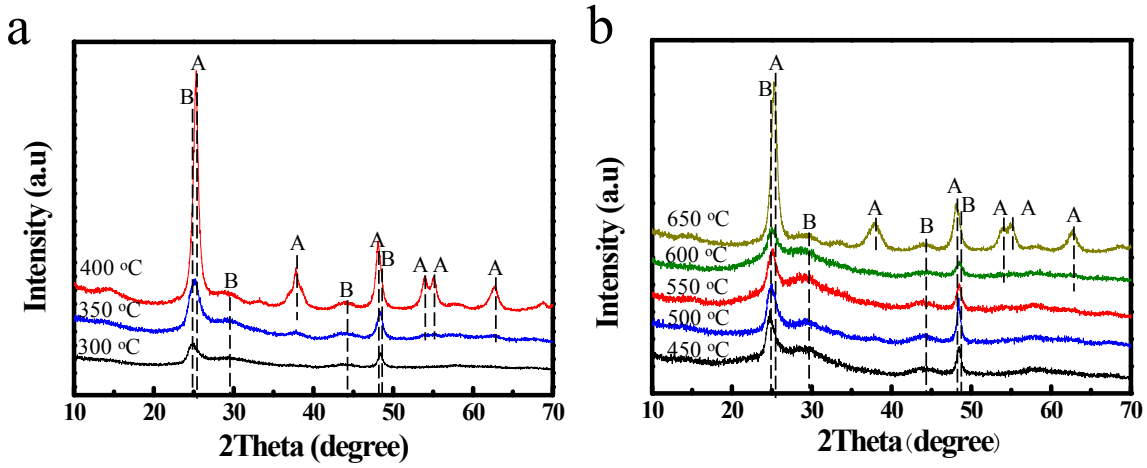

Fig. S4 XRD of (a) pristine TiO_2(B) and (b) B-TiO_2(B)-P annealing at different temperature under Ar armosphere. A: antase TiO_2 and B: TiO_2(B)

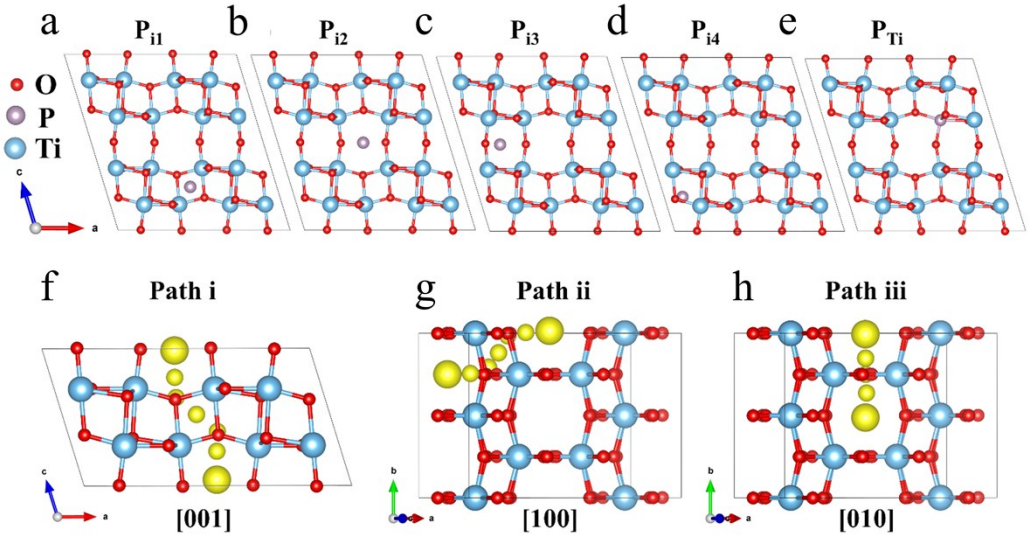

Fig. S5 (a)-(e) Possible P doping sites of interstitial P and P substitutional for Ti in bulk TiO_2(B). (f)-(h) Schematic diagram of three typical Na^+ diffusion paths along the [001], [100] and [010] directions, respectively.

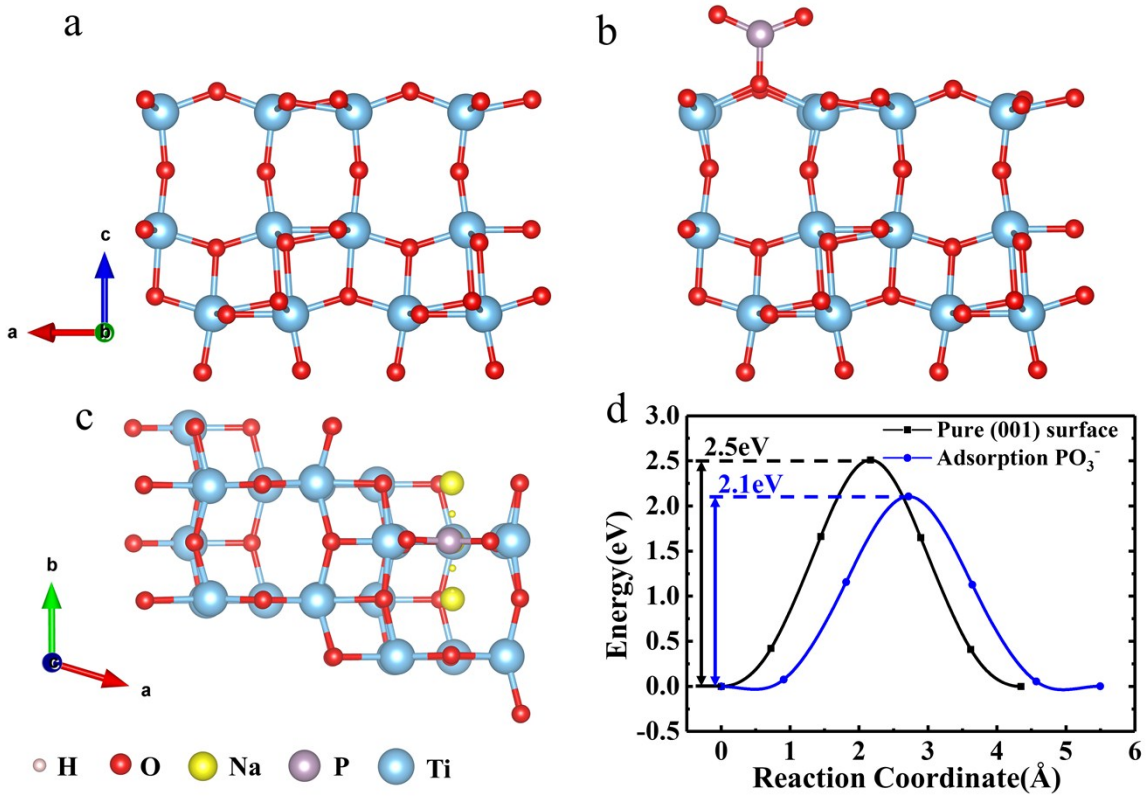

Fig. S6 The crystal structure of (001) surface for (a) pure TiO_2(B) and (b) TiO_2(B) with $(PO_3)^-$ adsorption. (c) Illustration top view of the Na diffusion along the [010] direction in TiO2(B) (001) surface with $(PO_3)^-$ adsorption. (d) Corresponding diffusion energy in pure and adsorbed $(PO_3)^-$ TiO_2(B) (001) surface.

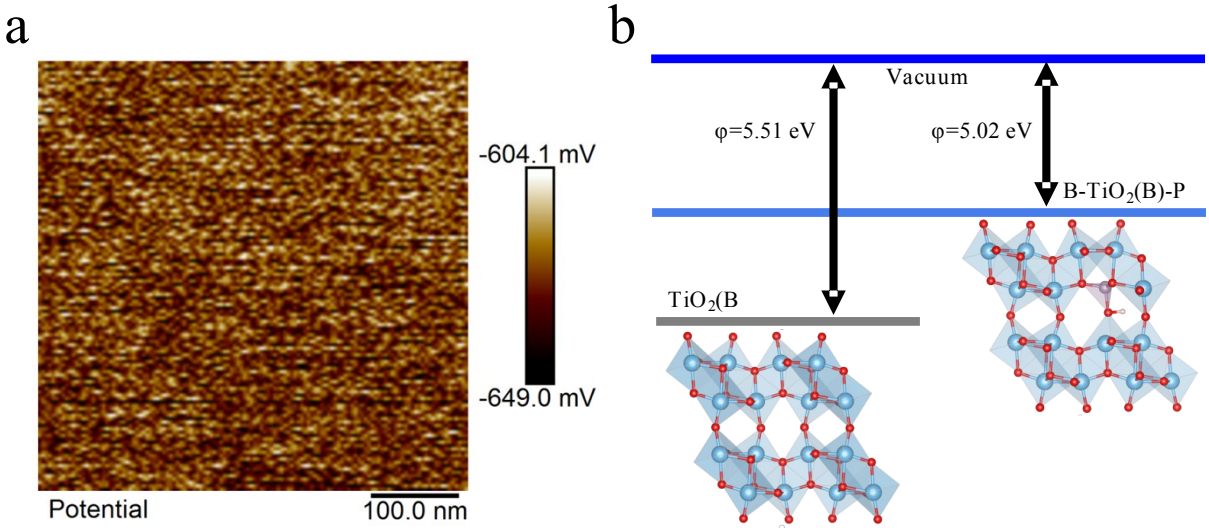

Fig.S7 (a) The surface potential map of Au foil (b) a diagrammatic drawing of Fermi level shift.

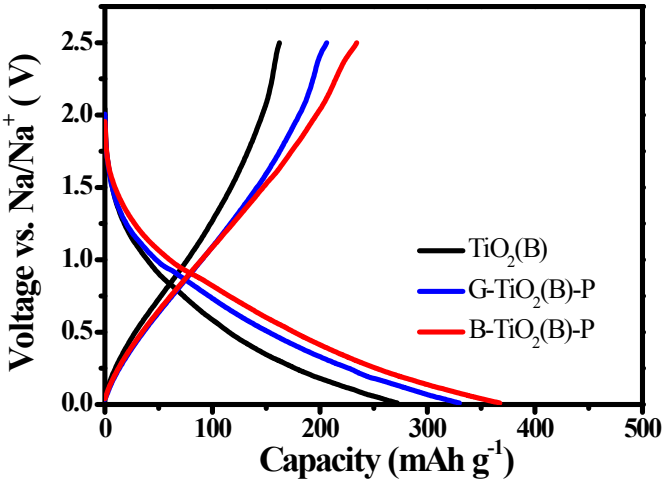

Fig.S8 Galvanostatic charge–discharge curves of the first cycle for different samples at the current density of 0.1 A g^{-1}.

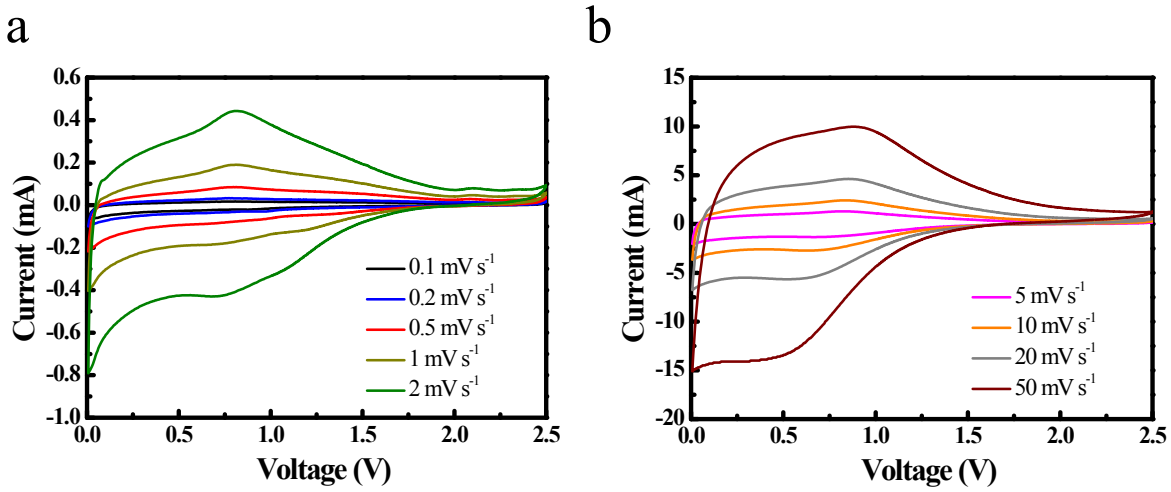

Fig. S9 Cyclic voltammetry curves of B-TiO_2(B)-P at various sweep rates: (a) 0.1-2 mV s^{-1} and (b) 5-50 mV s^{-1}.

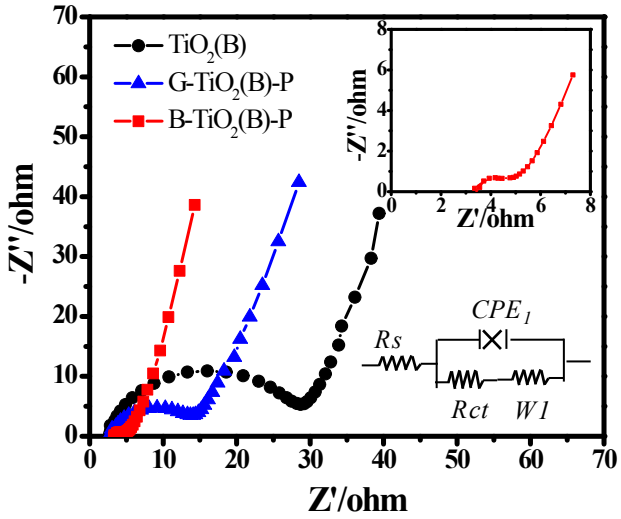

Samples	R_s(Ω)	R_{ct}(Ω)
TiO_2(B)	2.7	27
G-TiO_2(B)-P	2.7	12
B-TiO_2(B)-P	3.2	2

R_s: electrolyte resistance. CPE_1: capacitance impedance

R_{ct}: impedance of the charge transfer reaction. W: Warburg impedance

Figure. S10 EIS plots of different electrodes.

Table S1. The formation energy of interstitial P and P substitutional for Ti in bulk TiO_2(B).

Configuration	P_{i1}	P_{i2}	P_{i3}	P_{i4}	P_{Ti}
E_f (eV)	4.43	3.01	3.64	3.62	0.51